Disclaimer

This note has not been internally reviewed by the DØ Collaboration. Results or plots contained in this note were only intended for internal documentation by the authors of the note and they are not approved as scientific results by either the authors or the DØ Collaboration. All approved scientific results of the DØ Collaboration have been published as internally reviewed Conference Notes or in peer reviewed journals.

DØ note 2577

LBL–37244

$W\gamma$ and $Z\gamma$ Production at Tevatron*,†

H. Aihara

Lawrence Berkeley Laboratory

Berkeley, California 94720

Abstract

We present results from CDF and DØ on $W\gamma$ and $Z\gamma$ productions in $p\bar{p}$ collisions at $\sqrt{s} = 1.8$ TeV. The goal of the analyses is to test the non-abelian self-couplings of the W, Z and photon, one of the most direct consequences of the $SU(2)_L \otimes U(1)_Y$ gauge symmetry. We present direct measurements of $WW\gamma$ couplings and limits on $ZZ\gamma$ and $Z\gamma\gamma$ couplings, based on $p\bar{p} \to \ell\nu\gamma + X$ and $p\bar{p} \to \ell\ell\gamma + X$ events, respectively, observed during the 1992–1993 run of the Fermilab Tevatron Collider.

INTRODUCTION

Direct measurement of the $WW\gamma$ gauge boson couplings is possible through study of $W\gamma$ production in $p\bar{p}$ collisions at $\sqrt{s} = 1.8$ TeV. The most general effective Lagrangian [1],

---

*Invited talk given at the International Symposium on Vector Boson Self–Interactions, UCLA, February 1–3, 1995.

†This work was supported by the Director, Office of Energy Research, Office of High Energy and Nuclear Physics, Division of High Energy Physics of the U.S. Department of Energy under Contract DE-AC03-76SF00098.

invariant under $U(1)_{EM}$, for the $WW\gamma$ interaction contains four coupling parameters, CP–conserving κ and λ, and CP–violating $\tilde{\kappa}$ and $\tilde{\lambda}$. The CP–conserving parameters are related to the magnetic dipole (μ_W) and electric quadrupole (Q_W^e) moments of the W boson, while the CP–violating parameters are related to the electric dipole (d_W) and the magnetic quadrupole (Q_W^m) moments: $\mu_W = (e/2m_W)(1+\kappa+\lambda)$, $Q_W^e = (-e/m_W^2)(\kappa-\lambda)$, $d_W = (e/2m_W)(\tilde{\kappa}+\tilde{\lambda})$, $Q_W^m = (-e/m_W^2)(\tilde{\kappa}-\tilde{\lambda})$ [2]. In the Standard Model (SM) the $WW\gamma$ couplings at the tree level are uniquely determined by the $SU(2)_L \otimes U(1)_Y$ gauge symmetry: $\kappa = 1$ ($\Delta\kappa \equiv \kappa - 1 = 0$), $\lambda = 0$, $\tilde{\kappa} = 0$, $\tilde{\lambda} = 0$. The direct and precise measurement of the $WW\gamma$ couplings is of interest since the existence of anomalous couplings, i.e. measured values different from the SM predictions, would indicate the presence of physics beyond the SM. A $WW\gamma$ interaction Lagrangian with constant, anomalous couplings violates unitarity at high energies, and, therefore, the coupling parameters must be modified to include form factors (e.g. $\Delta\kappa(\hat{s}) = \Delta\kappa/(1+\hat{s}/\Lambda_W^2)^n$, where $\hat{s}$ is the square of the invariant mass of the W and the photon, Λ_W is the form factor scale, and $n = 2$ for a dipole form factor) [3].

The study of the $Z\gamma$ production in $p\bar{p}$ collision is also an important test of the SM description of gauge-boson self-interactions. Since the photon does not couple directly to the Z in the SM, this study is sensitive to anomalous couplings beyond the SM. The most general $ZZ\gamma$ ($Z\gamma\gamma$) vertex function is characterized by a set of four coupling parameters $h_{1-4}^{Z(\gamma)}$ [1]. All these coupling parameters vanish at tree level within the framework of the SM. The couplings h_3^V and h_4^V conserve CP, while h_1^V and h_2^V are CP-violating. Similarly to the $WW\gamma$ anomalous couplings, the $ZZ\gamma(Z\gamma\gamma)$ couplings must be regulated by generalized dipole form factors: $(h_i^V(\hat{s}) = h_{i0}^V/(1+\hat{s}/\Lambda_Z^2)^n$, where h_{i0}^V represents the low energy ($\hat{s} = 0$) limit for the couplings, and $n = 3$ for $h_{1,3}^V$ and $n = 4$ for $h_{2,4}^V$. Here the values for n were chosen so that the unitarity is preserved and that all terms in the matrix element proportional to h_{i0}^V have the same asymptotic energy behavior. At the Tevatron, the $W\gamma$ production is insensitive to the form factor effects for $\Lambda_W >$ a few 100 GeV, whereas the form factor effects cannot be ignored for $Z\gamma$ production due to the higher power of $\hat{s}$ dependence in the $ZZ\gamma(Z\gamma\gamma)$ vertex function.

We present studies of the $WW\gamma$ and $ZZ\gamma(Z\gamma\gamma)$ couplings based on $p\bar{p} \rightarrow \ell\nu\gamma + X$ and $p\bar{p} \rightarrow \ell\ell\gamma$ ($\ell = e, \mu$) events observed with the CDF [4] and DØ detector [5] during the 1992–1993 run of the Fermilab Tevatron Collider, corresponding to integrated luminosities of ~ 20 pb^{-1} for CDF and ~ 14 pb^{-1} for DØ. The $\ell\nu\gamma$ events contain the $W\gamma$ production process, $p\bar{p} \rightarrow W\gamma + X$ followed by $W \rightarrow \ell\nu$, and the radiative $W \rightarrow \ell\nu\gamma$ decay where the photon originates from bremsstrahlung of the charged lepton. Anomalous coupling parameters enhance the $W\gamma$ production with a large $\hat{s}$, and thereby result in an excess of events with high transverse energy, E_T, photons, well separated from the charged lepton. The $\ell\ell\gamma$ events contain the radiative $Z \rightarrow \ell\ell\gamma$ decay, the direct $Z\gamma$ production where the photon is radiated from one of the annihilating quarks, and the possible $Z\gamma$ events due to the anomalous Z-γ couplings. The presence of the Z-γ couplings will also be signaled by an excess of Z production with high E_T photons.

PHOTON DETECTION AT CDF AND DØ

Since the good detection of the photon is the key to the $W\gamma$ and $Z\gamma$ measurements, we briefly review how photons are detected by the CDF and DØ detectors. A photon is identified as a calorimeter energy cluster satisfying the following condition. A calorimeter cluster must (i) have a high electromagnetic energy fraction; (ii) be isolated; (iii) have shower shape consistent with a single photon; and (iv) have no tracks pointing to it. Table 1 summarizes the actual conditions required by CDF and DØ.

To test shower shape of the cluster CDF uses the central electromagnetic strip chambers [6] (CES) placed after ~ 6.3 radiation lengths in the central electromagnetic calorimeter. The CES determines shower position and transverse development of an electromagnetic shower at shower maximum by measurement of the charge deposition on orthogonal, fine-grained (1.5 cm spacing) strips and wires. DØ tests both longitudinal and transverse shower shapes including correlations between energy deposits in the fine-grained calorimeter cells [7]. The DØ electromagnetic calorimeter module has 4 longitudinal layers. Each of layers 1, 2

and 4 is segmented transversely to $\Delta\eta \times \Delta\phi = 0.1 \times 0.1$, while the third layer, which typically contains 65% of the EM energy, has segmentation of $\Delta\eta \times \Delta\phi = 0.05 \times 0.05$. ($\eta$ is the pseudorapidity defined as $\eta = -\ln(\tan(\theta/2))$, θ being the polar angle with repect to the beam axis. ϕ is the azimuthal angle.)

Both CDF and DØ found that the detection efficiency for photons depends on E_T^γ due to the isolation requirement. DØ found its cluster shape requirement also results in the E_T dependence. The overall photon detection efficiency was obtained by combining this E_T–dependent efficiency with the probabilities of losing a photon due to e^+e^- pair conversions and due to an overlap with a random track in the event. Table 2 summarizes the photon detection efficiencies at CDF and DØ.

$W\gamma$ ANALYSIS

The $W\gamma$ candidates were obtained by searching for events containing an isolated lepton (e or μ) with high E_T, large missing transverse energy, $\not\!\!E_T$, and an isolated photon. Table 3 summarizes geometrical and kinematic selection as well as integrated luminosity used in each channel. Both CDF and DØ required that the separation between a photon and a lepton be $\Delta R_{\ell\gamma} > 0.7$. This requirement suppresses the contribution of the radiative W decay process. The CDF observed 18 $W(e\nu)\gamma$ candidates and 7 $W(\mu\nu)\gamma$ candidates [8], while the DØ observed 11 $W(e\nu)\gamma$ candidates and 12 $W(\mu\nu)\gamma$ candidates [9].

The background estimate, summarized in Table 4, includes contributions from: W+jets, where a jet is misidentified as a photon; $Z\gamma$, where the Z decays to $\ell^+\ell^-$, and one of the leptons is undetected or is mismeasured by the detector and contributes to $\not\!\!E_T$; $W\gamma$ with $W \to \tau\nu$ followed by $\tau \to \ell\nu\bar{\nu}$. The W+jets background was estimated using the probability, $\mathcal{P}(j \to \text{“}\gamma\text{”})$, for a jet to be misidentified as a photon determined as a function of E_T of the jet by measuring the fraction of jets in a sample of multijet events that pass our photon identification requirements. For the photon criteria used by CDF, $\mathcal{P}(j \to \text{“}\gamma\text{”}) \sim 8 \times 10^{-4}$ at $E_T^j = 9$ GeV, decreasing exponentially to $\mathcal{P}(j \to \text{“}\gamma\text{”}) \sim 1 \times 10^{-4}$ at $E_T^j = 25$ GeV. For

TABLE I. Summary of photon detection at CDF and DØ

	CDF	DØ
detection region	$\|\eta\| < 1.1$ ($1.1 < \|\eta\| < 2.4$ [a])	$\|\eta\| < 1.1$ $1.5 < \|\eta\| < 2.5$
minimum E_T^γ	7 GeV	10 GeV
EM fraction	HAD/EM $< 0.055 + 0.00045 \times E(\text{GeV})$	$EM/Total > 0.9$
Isolation	$(E_T(0.4) - E_T^\gamma)/E_T^\gamma < 0.15$ [b] $p_T(0.4) < 2$ GeV/c	$(E(0.4) - EM(0.2))/EM(0.2) < 0.10$ [c]
Shower shape	transverse	longitudinal/transverse
No track	No matching tracks	No matching tracks

[a] Analysis in progress.

[b] $E_T(0.4)$ is the E_T in a cone of $\Delta R = \sqrt{(\Delta\eta)^2 + (\Delta\phi)^2} = 0.4$ around the photon candidate. $p_T(0.4)$ is the sum of p_T of the charged tracks within the same cone.

[c] $E(0.4)$ is the total energy inside a cone of radius $\Delta R = 0.4$, and $EM(0.2)$ is the EM energy inside a cone of 0.2.

TABLE II. Summary of photon detection efficiency.

	CDF	DØ	
	$\|\eta\| < 1.1$	$\|\eta\| < 1.1$	$1.5 < \|\eta\| < 2.5$
$E_T^\gamma > 25$ GeV	0.804 ± 0.023	0.74 ± 0.07	0.58 ± 0.05
$= 10$		0.43 ± 0.04	0.38 ± 0.03
$= 7$	0.731 ± 0.021		

TABLE III. Summary of $W\gamma$ event selection.

	CDF		DØ	
	$e\nu\gamma$	$\mu\nu\gamma$	$e\nu\gamma$	$\mu\nu\gamma$
Geometry	$\|\eta_e\| < 1.1$	$\|\eta_\mu\| < 0.6$	$\|\eta_e\| < 1.1$	$\|\eta_\mu\| < 1.7$
			$1.5 < \|\eta_e\| < 2.5$	
	$\|\eta_\gamma\| < 1.1$		$\|\eta_\gamma\| < 1.1, 1.5 < \|\eta_\gamma\| < 2.5$	
Kinematics	$E_T^e > 20$	$p_T^\mu > 20$	$E_T^e > 25$	$p_T^\mu > 15$
(in GeV)	$\not\!\!E_T > 20$	$\not\!\!E_T > 20$	$\not\!\!E_T > 25$	$\not\!\!E_T > 15$
	$E_T^\gamma > 7$		$E_T^\gamma > 10$	
	$\Delta R_{\ell\gamma} > 0.7$		$\Delta R_{\ell\gamma} > 0.7$	
$\int Ldt$ pb^{-1}	19.6 ± 0.7	18.6 ± 0.7	13.8 ± 0.7	13.7 ± 0.7

TABLE IV. Summary of $W\gamma$ data and backgrounds.

	CDF		DØ	
	$e\nu\gamma$	$\mu\nu\gamma$	$e\nu\gamma$	$\mu\nu\gamma$
Source:				
W+jets	4.6 ± 1.8	1.9 ± 0.6	1.7 ± 0.9	1.3 ± 0.7
$Z\gamma$	0.43 ± 0.02	1.14 ± 0.06	0.11 ± 0.02	2.7 ± 0.8
$W(\tau\nu)\gamma$	0.29 ± 0.02	0.15 ± 0.01	0.17 ± 0.02	0.4 ± 0.1
Total background	5.3 ± 1.8	3.2 ± 0.6	2.0 ± 0.9	4.4 ± 1.1
Data	18	7	11	12
Signal	12.7 ± 4.6	3.8 ± 2.7	$9.0^{+4.2}_{-3.1} \pm 0.9$	$7.6^{+4.4}_{-3.2} \pm 1.1$

TABLE V. Comparison of data and the SM prediction for $W\gamma$.

	CDF		DØ	
	$e\nu\gamma$	$\mu\nu\gamma$	$e\nu\gamma$	$\mu\nu\gamma$
Signal	12.7 ± 4.6	3.8 ± 2.7	$9.0^{+4.2}_{-3.1} \pm 0.9$	$7.6^{+4.4}_{-3.2} \pm 1.1$
SM prediction	15.4 ± 0.7	7.9 ± 0.4	6.9 ± 1.0	6.7 ± 1.2
$\sigma_{W\gamma}$ ($E_T^\gamma >$ 7GeV,$\Delta R_{\ell\gamma} > 0.7$) pb	141.7 ± 53	83 ± 59		
$\sigma_{W\gamma}$ ($E_T^\gamma > 10$GeV,$\Delta R_{\ell\gamma} > 0.7$) pb			147^{+73}_{-56}	127^{+78}_{-61}
$e + \mu$ combined	122 ± 42 pb		138^{+55}_{-43} pb	
SM prediction	172 ± 26 pb		112 ± 10 pb	

the photon criteria used by DØ, $\mathcal{P}(j \rightarrow \text{“}\gamma\text{”}) \sim 4 \times 10^{-4}$ (6×10^{-4}) in the central (endcap) calorimeter, and varies only slowly with E_T^j. The total number of W+jets background events was calculated by applying $\mathcal{P}(j \rightarrow \text{“}\gamma\text{”})$ to the observed E_T spectrum of jets in the inclusive $W(\ell\nu)$ sample. The backgrounds due to $Z\gamma$ and $W \rightarrow \tau\nu$ were estimated from Monte Carlo simulations.

The kinematic and geometrical acceptance was calculated as a function of coupling parameters, $\Delta\kappa$ and λ, using the Monte Carlo program of Baur and Zeppenfeld, in which the $W\gamma$ production and radiative decay processes are generated to leading order, and higher order QCD effects are approximated by a K-factor. Both CDF and DØ used the MRSD_' structure functions and simulated the p_T distribution of the $W\gamma$ system using the observed p_T spectrum of the W in the inclusive $W(\ell\nu)$ sample. The generated events underwent a detector simulation. Table 5 shows the comparison between the observed signal and the SM prediction. CDF obtained the $W\gamma$ cross section for photons with $E_T^\gamma > 7$ GeV and $\Delta R_{\ell\gamma} > 0.7$ from a combined $e + \mu$ sample: $\sigma(W\gamma) = 122 \pm 42$ pb, while the SM predicts 172 ± 26 pb. DØ obtained $\sigma(W\gamma) = 138^{+55}_{-43}$ pb for photons with $E_T^\gamma > 10$ GeV and $\Delta R_{\ell\gamma} > 0.7$, and the SM predicts 112 ± 10 pb. Here we used BR$(W \rightarrow \ell\nu) = 0.108$. The observed cross section agrees with the SM prediction within errors.

Figures 1 and 2 show that data and the SM prediction plus the background in the distributions of E_T^γ, $\Delta R_{\ell\gamma}$, and the cluster transverse mass defined by $M_T(\gamma\ell;\nu) = (((m_{\gamma\ell}^2 + |\mathbf{E_T^\gamma} + \mathbf{E_T^\ell}|^2)^{\frac{1}{2}} + \not\!\!E_T)^2 - |\mathbf{E_T^\gamma} + \mathbf{E_T^\ell} + \not\!\!\mathbf{E_T}|^2)^{\frac{1}{2}}$. Of 25 events CDF observed, 16 events having $M_T(\gamma\ell;\nu) \leq M_W$ are primarily the radiative W decay events plus background. Similarly, of 23 events DØ observed, 11 events are primarily the radiative W decay events plus background. The absence of an excess of high E_T photons rules out deviations from the SM couplings.

To set limits on the anomalous coupling parameters, a binned maximum likelihood fit was performed on the E_T^γ spectrum for each of the $W(e\nu)\gamma$ and $W(\mu\nu)\gamma$ samples, by calculating the probability for the sum of the Monte Carlo prediction and the background to fluctuate to the observed number of events. The uncertainties in background estimate, efficiencies,

acceptance and integrated luminosity were convoluted in the likelihood function with Gaussian distributions. A dipole form factor with a form factor scale $\Lambda_W = 1.5$ TeV was used in the Monte Carlo event generation. The limit contours for the CP–conserving anomalous coupling parameters $\Delta\kappa$ and λ are shown in Fig. 3, assuming that the CP–violating anomalous coupling parameters $\tilde{\kappa}$ and $\tilde{\lambda}$ are zero. For comparison, previous limits obtained by UA2 and CDF from the 1988-89 data are included. Current limits on CP–conserving anomalous $WW\gamma$ couplings are:

$$\text{CDF} \quad -2.3 < \Delta\kappa < 2.3 \ (\lambda = 0), \quad -0.7 < \lambda < 0.7 \ (\Delta\kappa = 0),$$

$$\text{D}\emptyset \quad -1.6 < \Delta\kappa < 1.8 \ (\lambda = 0), \quad -0.6 < \lambda < 0.6 \ (\Delta\kappa = 0),$$

at the 95% confidence level. Limits on CP–violating coupling parameters were within $3-6\%$ of those obtained for $\Delta\kappa$ and λ. It was found that the limits are insensitive to the form factor for $\Lambda_W > 200$ GeV and are well within the constraints imposed by the S-matrix unitarity [10] with $\Lambda_W = 1.5$ TeV. DØ also performed a two dimensional fit including $\Delta R_{\ell\gamma}$, and found that the results are within 3% of those obtained from a fit to the E_T^γ spectrum only.

$Z\gamma$ ANALYSIS

The $Z\gamma$ candidates were obtained by searching for events containing two isolated, high E_T, leptons, and an isolated photon. Table 6 summarizes geometrical and kinematic selection as well as integrated luminosity used in each channel. The CDF observed 4 $ee\gamma$ candidates and 4 $\mu\mu\gamma$ candidates [11], while the DØ observed 4 $ee\gamma$ candidates and 2 $\mu\mu\gamma$ candidates [12]. The background estimate, summarized in Table 7, includes contributions from: Z+jets, where a jet is misidentified as a photon; $Z\gamma$ with $Z \rightarrow \tau\tau$. Because we require three isolated objects in the final state, the background in the $Z\gamma$ candidates is small.

TABLE VI. Summary of $Z\gamma$ event selection.

	CDF		DØ	
	$ee\gamma$	$\mu\mu\gamma$	$ee\gamma$	$\mu\mu\gamma$
Geometry	$\lvert\eta_{e1}\rvert < 1.1$	$\lvert\eta_{\mu1}\rvert < 0.6$	$\lvert\eta_{e1,2}\rvert < 1.1$	$\lvert\eta_{\mu1,2}\rvert < 1.0$
	$1.1 < \lvert\eta_{e2}\rvert < 4.2$	$\lvert\eta_{\mu2}\rvert < 1.2$	$1.5 < \lvert\eta_{e1,2}\rvert < 2.5$	
	$\lvert\eta_\gamma\rvert < 1.1$		$\lvert\eta_\gamma\rvert < 1.1,\ 1.5 < \lvert\eta_\gamma\rvert < 2.5$	
Kinematics	$E_T^{e1} > 20$	$p_T^{\mu1,2} > 20$	$E_T^{e1,2} > 25$	$p_T^{\mu1} > 15$
(in GeV)	$E_T^{e2} > 20, 15, 10$			$p_T^{\mu2} > 8$
	$E_T^\gamma > 7$		$E_T^\gamma > 10$	
	$\Delta R_{\ell\gamma} > 0.7$		$\Delta R_{\ell\gamma} > 0.7$	
$\int Ldt$ pb^{-1}	19.7 ± 0.7	18.6 ± 0.7	13.9 ± 1.7	13.3 ± 1.6

The background–subtracted signal agrees well with the SM prediction calculated using the Monte Carlo program of Baur and Berger. CDF derived the $Z\gamma$ cross section times $Z \to \ell\ell$ branching ratio for photons with $\Delta R_{\ell\gamma} > 0.7$ and $E_T^\gamma > 7$ GeV from a combined $e + \mu$ sample: $\sigma(Z\gamma) \cdot Br(Z \to \ell\ell) = 5.1 \pm 1.9(stat) \pm 0.3(syst)$ pb, in good agreement with the SM prediction of $5.2 \pm 0.6(stat \oplus syst)$ pb. Figure 4 and 5 show the data and the SM prediction plus the background in the distributions of E_T^γ and $\ell^+\ell^-\gamma$ invariant mass for CDF, and E_T^γ for DØ , respectively. No significant deviation from the SM prediction was observed.

Similarly to the $W\gamma$ analysis, limits on anomalous $Z\gamma$ couplings were obtained by a fit to the E_T^γ spectrum. Figure 6 shows the current CDF and DØ 95% limit contours for anomalous $ZZ\gamma$ couplings together with the limits from L3 [13] experiment and the constraints

TABLE VII. Summary of $Z\gamma$ data, backgrounds and the SM predictions.

	CDF		DØ	
	$ee\gamma$	$\mu\mu\gamma$	$ee\gamma$	$\mu\mu\gamma$
Source:				
Z+jets	0.4 ± 0.2	0.1 ± 0.1	0.43 ± 0.06	0.02 ± 0.01
$Z(\tau\tau)\gamma$	negligible	negligible	negligible	0.03 ± 0.01
Total background	0.4 ± 0.2	0.1 ± 0.1	0.43 ± 0.06	0.05 ± 0.01
Data	4	4	4	2
Signal	3.6 ± 2.0	3.9 ± 2.0	$3.6^{+3.2}_{-1.9}$	$1.95^{+2.6}_{-1.3}$
SM prediction	4.3 ± 0.2	2.8 ± 0.1	3.2 ± 0.5	2.5 ± 0.5

from S-matrix unitarity for $\Lambda_Z = 500$ GeV. The pair of h_{30}^Z and h_{40}^Z is CP–conserving, while that of h_{10}^Z and h_{20}^Z is CP–violating. Limits on CP–conserving $ZZ\gamma$ couplings are:

$$\text{CDF} \quad -3.0 < h_{30}^Z < 2.9 \ (h_{40}^Z = 0), \quad -0.7 < h_{40}^Z < 0.7 \ (h_{30}^Z = 0),$$

$$\text{DØ} \quad -1.9 < h_{30}^Z < 1.8 \ (h_{40}^Z = 0), \quad -0.5 < h_{40}^Z < 0.5 \ (h_{30}^Z = 0),$$

at the 95% confidence level. Limits on $Z\gamma\gamma$ couplings are the same to within 0.1. The sensitivity of limits to the form factor scale, Λ_Z, was studied. Both CDF and DØ data reach the limit set by unitarity for $\Lambda_Z \sim 500$ GeV, which can be interpreted as the sensitivity limit from the current data.

CONCLUSION

In conclusion, CDF and DØ has studied $W\gamma$ and $Z\gamma$ productions at $\sqrt{s} = 1.8$ TeV in electron and muon channels. The observed photon E_T spectra agree well with the standard model predictions, yielding limits on anomalous $WW\gamma$, $ZZ\gamma$ and $Z\gamma\gamma$ couplings.

It is a pleasure to thank the members of the organizing committee, U. Baur, S. Errede and T. Müller, and the conference staff for running the conference so smoothly. I am indebted to my colleagues on DØ and the members of CDF electroweak physics group for their help in preparing the talk. This work was supported by the Director, Office of Energy Research, Office of High Energy and Nuclear Physics, Division of High Energy Physics of the U.S. Department of Energy under Contract DE-AC03-76SF00098.

REFERENCES

[1] K. Hagiwara, R.D. Peccei, D. Zeppenfeld and K. Hikasa, Nucl. Phys. **B282**, 253 (1987).

[2] K. Kim and Y-S. Tsai, Phys. Rev. D **7**, 3710 (1973).

[3] U. Baur and E.L. Berger, Phys. Rev. D **41**, 1476 (1990).

[4] CDF Collaboration, F. Abe *et al.*, Nucl. Instrum. Methods **A271**, 387 (1988).

[5] DØ Collaboration, S. Abachi *et al.*, Nucl. Instrum. Methods **A338**, 185 (1994).

[6] CDF Collaboration, F. Abe *et al.*, Fermilab-PUB-94-244-E. To appear in Phys. Rev. D.

[7] DØ Collaboration, M. Narain, "Proceedings of the American Physical Society Division of Particles and Fileds Meeting," Fermilab (1992), eds. R. Raja and J. Yoh, Vol.2, 1678.

[8] CDF Collaboration, F. Abe *et al.*, Phys. Rev. Lett. **74**, 1936 (1995).

[9] DØ Collaboration, S. Abachi *et al.*, Fermilab-PUB-95-101-E, Submitted to Phys. Rev. Lett.

[10] U. Baur and D. Zeppenfeld, Phys. Lett. **B201**, 383 (1988).

[11] CDF Collaboration, F. Abe *et al.*, Phys. Rev. Lett. **74**, 1941 (1995).

[12] G. Landsberg, these proceedings; DØ Collaboration, S. Abachi *et al.*, Fermilab-PUB-95-042-E. Submitted to Phys. Rev. Lett.

[13] P. Mattig, these proceedings; O. Adrianni *et. al*, Phys. Lett. **B345**, 609 (1995).

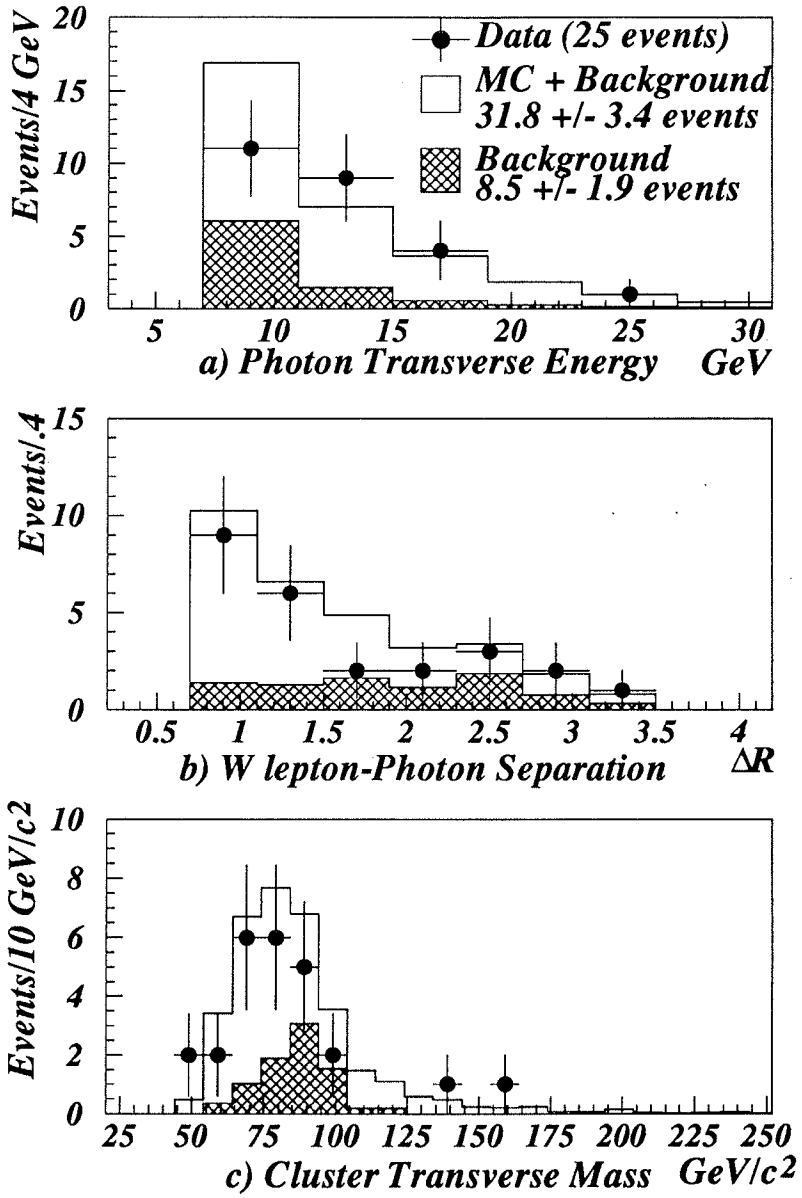

FIG. 1. CDF Distribution of (a) E_T^γ, (b) $\mathcal{R}_{\ell\gamma}$ and (c) $M_T(\gamma\ell;\nu)$ for the $W(e\nu)\gamma + W(\mu\nu)\gamma$ combined sample. The points are data. The shaded areas represent the estimated background, and the solid histograms are the expected signal from the Standard Model plus the estimated background.

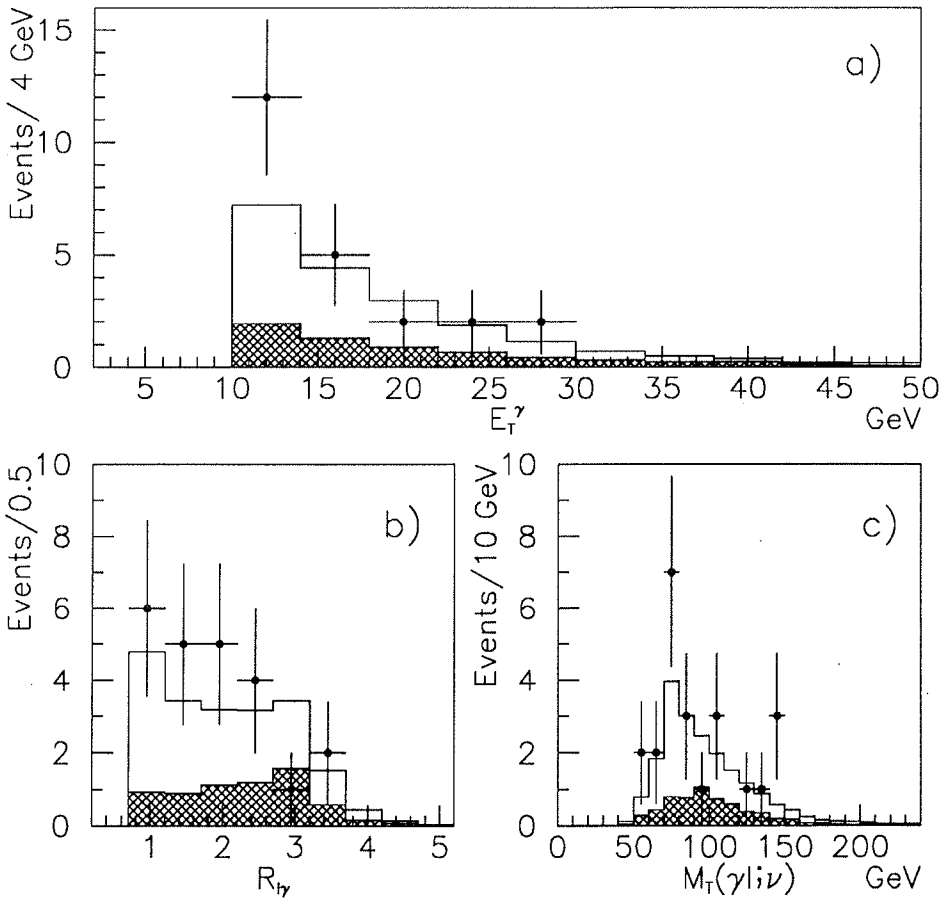

FIG. 2. DØ Distribution of (a) E_T^γ, (b) $\mathcal{R}_{\ell\gamma}$ and (c) $M_T(\gamma\ell;\nu)$ for the $W(e\nu)\gamma + W(\mu\nu)\gamma$ combined sample. The points are data. The shaded areas represent the estimated background, and the solid histograms are the expected signal from the Standard Model plus the estimated background.

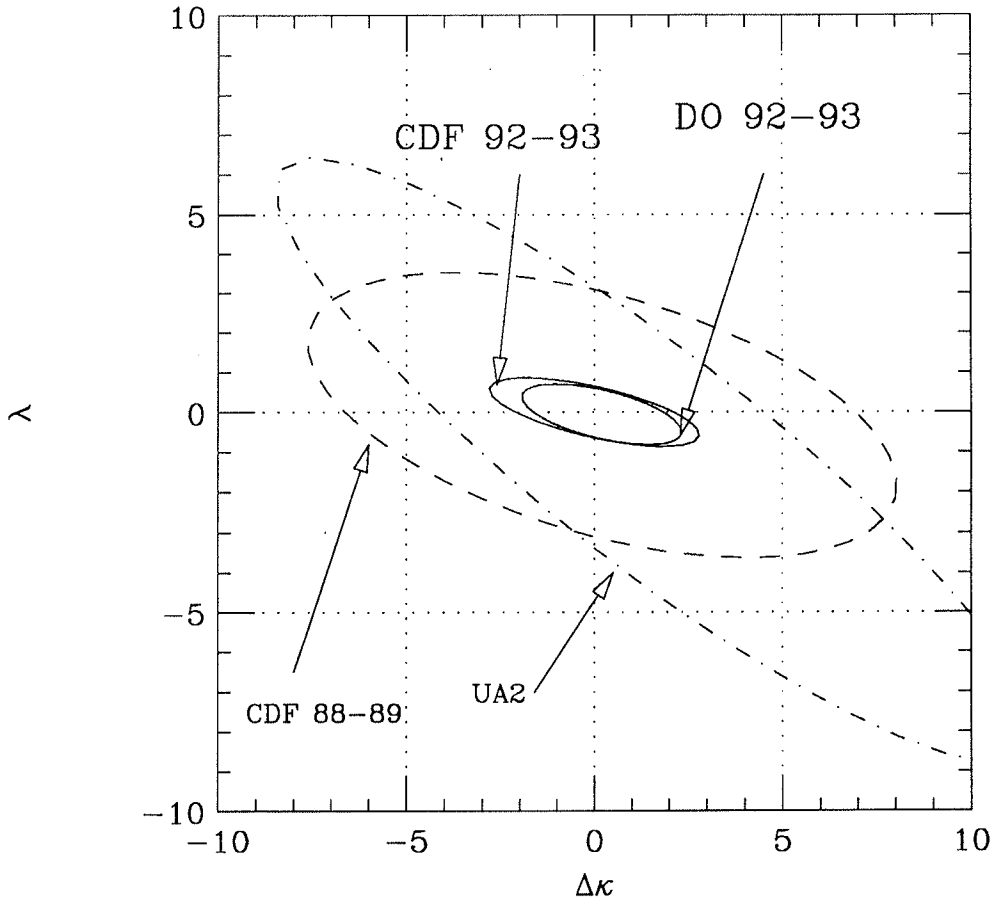

FIG. 3. Limits on CP–conserving anomalous coupling parameters $\Delta\kappa$ and λ. The ellipses represent the 95% exclusion contours. Present limits from CDF and DØ are shown together with previous limits.

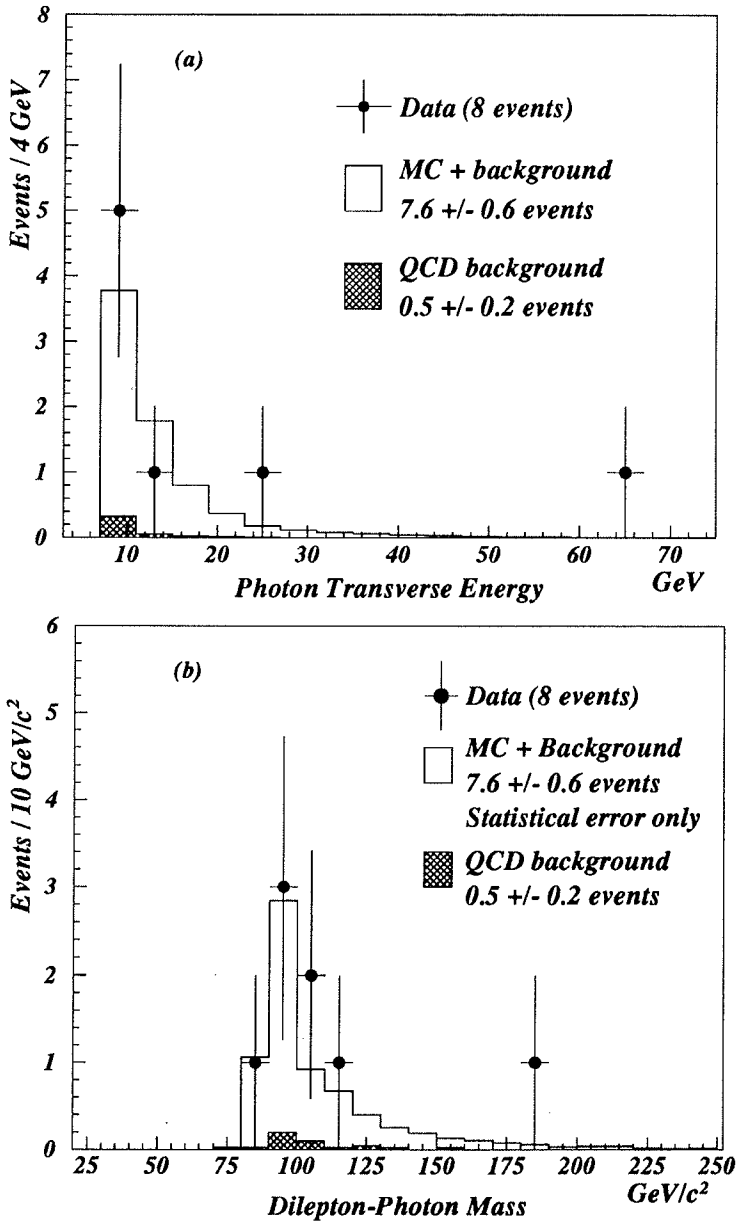

FIG. 4. CDF Distributions of (a) E_T^γ and (b) the $\ell^+\ell^-\gamma$ invariant mass. for electron and muon channels combined. The points are data. The shaded areas represent the estimated background, and the solid histograms are the expected signal from the Standard Model plus the estimated background.

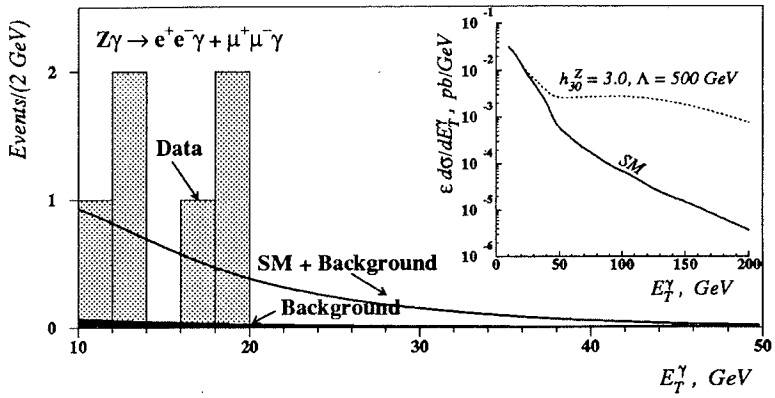

FIG. 5. DØ Distributions of (a) E_T^γ of $ee\gamma$ and $\mu\mu\gamma$ events. The histogram corresponds to the data, the shaded area represents the estimated background, and the solid line shows the sum of the SM prediction and the background. The insert shows $d\sigma/dE_T^\gamma$ folded with efficiencies for the SM and anomalous ($h_{30}^Z = 3.0$) couplings.

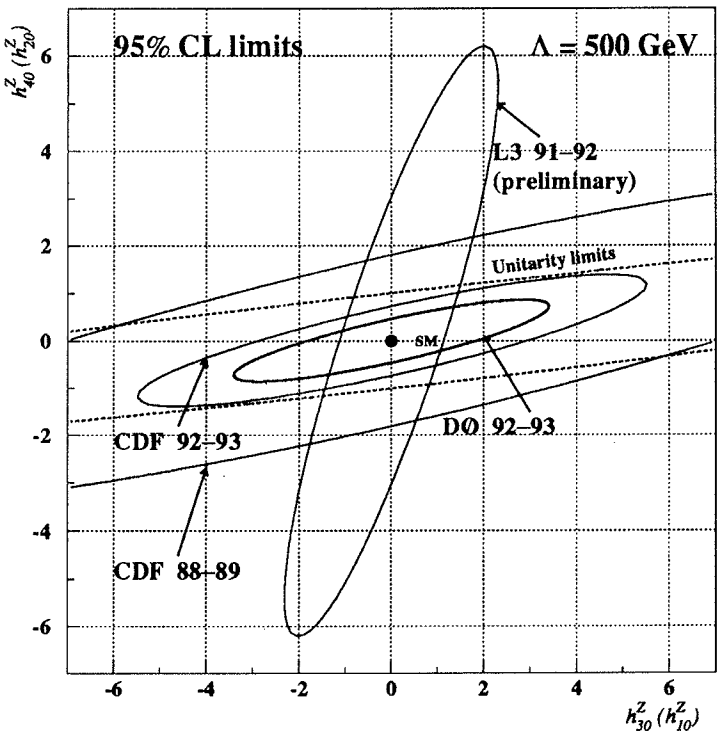

FIG. 6. Comparison of the limits on the CP–conserving (CP–violating) anomalous $ZZ\gamma$ coupling parameters h_{30}^Z and h_{40}^Z (h_{10}^Z and h_{20}^Z). The solid ellipses represent 95% CL exclusion contours for DØ , CDF and L3 experiments. The dashed curve shows limits from unitarity for the form factor scale of $\Lambda_Z = 500$ GeV.